

## Atomic Carbon in Galaxies

Maryvonne Gerin,<sup>1,2</sup> Thomas G. Phillips,<sup>3</sup>

Received \_\_\_\_\_; accepted \_\_\_\_\_

---

<sup>1</sup>Radioastronomie millimétrique - UMR 8540 du CNRS, Laboratoire de Physique de l'ENS, 24 Rue Lhomond, 75231 Paris cedex 05, France.

maryvonne.gerin@physique.ens.fr

<sup>2</sup>DEMIRM - UMR 8540 du CNRS, Observatoire de Paris, 61 Avenue de l'Observatoire 75014 Paris, France

<sup>3</sup>Caltech Submillimeter Observatory, Caltech 320-47, Pasadena, CA 91125.  
phillips@submm.caltech.edu

## ABSTRACT

We present new measurements of the ground state fine-structure line of atomic carbon at 492 GHz in a variety of nearby external galaxies, ranging from spiral to irregular, interacting and merging types. In comparison with CO(1-0) emission observed at the same spatial resolution, the CI(1-0) line intensity stays fairly comparable in the different environments, with an average value of the ratio of the line integrated areas in  $\text{Kkm s}^{-1}$  of  $\text{CI(1-0)}/\text{CO(1-0)} = 0.2 \pm 0.2$ . However, some variations can be found within galaxies, or between galaxies. Relative to CO lines ( $J=2-1, 3-2, 4-3$ ), CI(1-0) is weaker in galactic nuclei, but stronger in disks, particularly outside star forming regions. Also, in NGC 891, the CI(1-0) emission follows the dust continuum emission at 1.3mm extremely well along the full length of the major axis where molecular gas is more abundant than atomic gas. Atomic carbon therefore appears to be a good tracer of molecular gas in external galaxies, possibly more reliable than CO.

Atomic carbon can contribute significantly to the thermal budget of interstellar gas. The cooling due to C and CO are of the same order of magnitude for most galaxies. However, CO is generally a more important coolant in starburst galaxies. Cooling due to C and CO amounts typically to  $2 \times 10^{-5}$  of the FIR continuum or 5% of the CII line. However, C and CO cooling reaches  $\sim 30\%$  of the gas total, in Ultra Luminous InfraRed Galaxies (ULIRG) like Arp 220, where CII is abnormally faint.

Together with CII/FIR, the emissivity ratio  $\text{CI(1-0)}/\text{FIR}$  can be used as a measure of the non-ionizing UV radiation field in galaxies. The plots of CII/CI or CII/FIR versus CI/FIR show good correlations, in agreement with PDR models, except for two remarkable galaxies Arp 220 and Mrk 231, where high opacities of the CII line and possibly the dust thermal emission may be factors

reducing the CII strength below the predictions of the current PDR models.

## 1. Introduction

Due to the poor transparency of the Earth’s atmosphere at submillimeter wavelengths, there are few published measurements of the ground state fine-structure lines of atomic carbon at 492 and 809 GHz in external galaxies, despite the high abundance of this species in cool interstellar gas and its importance for the overall thermal budget of molecular gas. The first detection was reported by Büttgenbach et al. (1992) in IC 342. A handful of galaxies have been detected since, including NGC 253 (Israel et al. 1995, Harrison et al. 1995), M 82 (Schilke et al. 1993, Stutzki et al. 1997), M 83 (Petitpas and Wilson 1998), M 33 (Wilson 1997). Individual clouds have been observed in M 31 (Israel et al. 1998) and the LMC (Stark et al. 1997).

Atomic carbon can be found in all types of neutral clouds, from diffuse clouds (Jenkins & Shaya 1979) to dense molecular gas (Phillips & Huggins 1981). In diffuse clouds, atomic carbon is a minor constituent, but the intensity ratio of the two ground state fine-structure lines is a sensitive tracer of the total gas pressure. Atomic carbon has also proven to be a good tracer of molecular gas in Galactic molecular clouds, as a linear correlation is commonly found between the strength of the CI( $^3P_1 - ^3P_0$ ) line at 492 GHz and the  $^{13}\text{CO}(2-1)$  line at 220 GHz (Keene et al. 1996). This correlation corresponds to a mean abundance of neutral carbon of  $\sim 10^{-5}$  relative to  $\text{H}_2$ . By comparing with extinction measurements, Frerking et al. (1989) found a similar value for the abundance of atomic carbon in dense molecular clouds, where it reaches a maximum of  $2.2 \times 10^{-5}$  for  $A_V = 4 - 11$  mag and does not deviate from this value by more than a factor of a few for larger  $A_V$ . Emission from the two ground state fine-structure lines of atomic carbon is seen by COBE throughout the Milky Way and makes a significant contribution to the gas cooling (Bennett

et al. 1994). Therefore, it is not surprising that these ubiquitous atomic carbon lines are present in the spectra of external galaxies.

From a theoretical point of view, the spatial distribution and line intensities of atomic carbon in molecular clouds are predicted by chemical models which include the effect of photodissociation induced by UV photons, the so-called PDR models (e.g. Tielens and Hollenbach 1985). In clouds exposed to UV radiation, carbon is mostly in the form of  $\text{C}^+$  to a depth  $\text{Av} = 1$  magnitude. Atomic carbon appears at an intermediate depth, from  $\text{Av} = 1$  to 5 or so magnitudes, where  $\text{C}^+$  is mostly recombined with electrons and not all the gas phase carbon present is yet captured into CO. The actual depth of this zone, and thus the extent and intensity of the CI emission, is a sensitive function of some important model parameters, such as the carbon and oxygen abundance in the gas phase, and the presence of Polycyclic Aromatic Hydrocarbons (see Bakes and Tielens 1998, Le Bourlot et al. 1993). PDR models are difficult to use for quantitative results in galaxies, because they were developed to represent the structure of an individual cloud, whereas a galaxy would have to be synthesized from a suitable ensemble of PDR clouds (see e.g. Sauty et al. 1998). Nevertheless, their predictions provide a qualitative understanding of the variations of the line flux with physical conditions. Previous CII measurements of external galaxies have been compared successfully with such PDR models (e.g. Stacey et al. 1991).

Although CII, CI and CO emission, in principle, arise from different physical regions in the cloud, in actual observations of Galactic clouds it is found that CI and CO emission on average seem to come from the same physical region. This is in part due to the clumpy or fractal nature of the clouds, so that the UV causes emission from irradiated regions even deep into the cloud. The overall

impression, at moderate (say 15" at 500 pc = 0.04 pc) resolution, is that the species are coexistent. This scale must be compared to the size of Galactic clouds, which may vary from a few parsecs to a few tens of parsecs. Few large scale maps of Galactic clouds have been made for all these species, but for some giant molecular clouds (Plume et al. 1994, 1999) there is a good correspondence between the CI, CII and CO maps. For external galaxies where individual clouds are barely resolved, we would then expect that the different carbon species will be observationally coexistent (when associated with molecular gas) including the ionized carbon. Therefore, at least for the point of view of beam dilution in the observations, the 3 species (CII, CI and CO) can be considered as occupying the same volume in the beam so that observed line ratios can be compared with model predictions. The ionized interstellar medium, either diffuse or in HII regions, can contribute to the global CII emission of galaxies, but for starforming regions in galaxies, PDRs contribute most of the CII emission (Madden et al. 1993, Sauty et al. 1998). For M 82 the contribution of HII regions is estimated to be  $\sim 24\% - 31\%$  of the observed CII flux (Colbert et al. 1999).

The contribution of the cool diffuse regions to the atomic carbon emission will be incorporated in the PDR models. The warm diffuse gas is generally ionized and therefore barely contributes to the CI emission. Therefore, the two fine-structure lines of atomic carbon are expected to be better tracers of PDRs than is CII. The intensity ratio  $CI(1-0)/CO(1-0)$  is a function of the gas density and UV illumination factor  $G_0$ , as shown in Figure 1, produced with the PDR model developed by Le Bourlot et al. (1993) and Abgrall et al. (1992).  $G_0$  is defined relative to the average interstellar radiation field in the solar neighborhood as obtained by Mathis et al. (1983)  $G_0 = I_{UV}(6-13.6 \text{ eV})/1.4 \times 10^{-4} \text{ erg cm}^{-2}\text{s}^{-1}\text{sr}^{-1}$ ;  $n_H$  represents the total density of hydrogen atoms.

Other ratios, CII/CI, CI/FIR and CII/FIR depend mostly on the UV illumination factor  $G_0$  (see also Kaufman et al. 1999). Since atomic carbon is present in a layer of the PDR with almost the same characteristics (column density, temperature) whatever the illumination, the brightness of the CI(1-0) line is fairly constant for most of the parameter space studied. This means that the main factor affecting this line in external galaxies is the filling factor of the emission in the beam. By contrast, the FIR emission in a PDR is directly proportional to the UV illumination since nearly all the incident UV radiation is absorbed in the cloud. Finally, the CII and OI emission in PDRs, depend on both the UV illumination (due to the decrease of the efficiency of photoelectric heating at high illumination) and the gas density (for the collisional excitation of these lines). From the PDR models, it is expected that the CI/FIR ratio will be a useful tracer of the local UV illumination conditions.

In the following we present new observations of CI(1-0), as well as complementary data,  $^{13}\text{CO}$ (2-1),  $^{12}\text{CO}$ (2-1), (3-2) and (4-3), on nearby galaxies, of various morphological types. These data are used to study the correlation of CI emission with other tracers of the ISM in galaxies.

## 2. Observations

The observations were performed with the Caltech Submillimeter Observatory (CSO) during 1996 - 1998, using SIS receivers operated in double-side (DSB) mode. In good atmospheric conditions ( $\tau_{225\text{GHz}} \leq 0.06$ ), the single sideband system temperature usually ranged between 1000 and 3000 K. The observations were performed using a chopping secondary mirror, with throw set to 1 to 3 arcminutes on the sky, depending on the size of the source. The spectra were analysed with two acousto-optic spectrometers, one with a total bandwidth

of 1500 MHz (of which only 900 MHz is used, due to the bandwidth limit of the receivers) and a resolution of about 2 MHz, and a second with a total bandwidth of 500 MHz and a spectral resolution of about 1.5 MHz. The main beam efficiencies of the CSO were 0.72, 0.65 and 0.53 at 230, 345 and 492 GHz respectively; the corresponding conversion factors between Janskys and Kelvins ( $T_A^*$ ) are 50, 70 and 100 Jy/K, and beam sizes 30 ", 20" and 15 ". Some data have been reported previously (Gerin & Phillips 1997, 1998). The program galaxies are listed in Table 1.

Most of the target galaxies have narrow lines which fit in a single backend spectrometer setting. For two galaxies with broad lines, Arp 220 and the center of NGC 3079, we used three different local oscillator settings to obtain a complete coverage of the lines, with central velocities at -300, 0 and +300  $\text{km s}^{-1}$  relative to the line center. First, we used the spectra taken at velocity offsets +300 and -300  $\text{km s}^{-1}$  to adjust the zero level of the baseline, with a window set by reference to published CO spectra. We then computed the baseline offset for the central spectrum, to minimize the platforming effects with the spectra taken at +300 and -300  $\text{km s}^{-1}$ . The overlap region is quite large, +70 to +200  $\text{km s}^{-1}$  at positive velocities for Arp 220 for example. The data and interpretation for Arp 220 have been reported elsewhere (Gerin & Phillips 1998).

### 3. Results

CI(1-0) was detected in all the program galaxies. Figure 2 presents a selection of CSO spectra. The measured parameters are listed in Table 2, together with complementary data found in the literature. Linear baselines have been fitted with the original spectral resolution ( $\sim 1.5 \text{ MHz} = 0.8 \text{ km s}^{-1}$ ). Depending on the expected line width, the spectra have then been rebinned to

$5 - 15 \text{ kms}^{-1}$  resolution to increase the S/N ratio. For galaxies with broad lines and not too many channels beyond the line, we chose the line window according to published CO spectra. The uncertainty in the line flux due to the uncertainty in the position of the baseline is included in the total uncertainty listed in Table 2. Figure 3 shows the integrated intensity ratio  $\text{CI}(1-0)/\text{CO}(1-0)$  in  $T_{mb}$  as a function of the  $\text{CO}(1-0)$  integrated intensity in  $\text{Kkm s}^{-1}$ . This ratio has a mean value of  $0.2 \pm 0.2$ , with a large dispersion, since the observed ratios range from  $\sim 0.04$  to  $\sim 1$ . To get the emissivity ratio, the observed intensity ratio in  $T_{mb}$  must be multiplied by 78, the cube of the ratio of the line frequencies. The mean emissivity ratio is therefore 16, with observed values ranging from 3 to 80. In this figure the  $\text{CO}(1-0)$  data are taken from the literature, as listed in Table 2. We also included any already published CI data. We used mostly the  $\text{CO}(1-0)$  data taken with the IRAM 30m telescope in order to match the CI beam size at the CSO as closely as possible. The  $\text{CO}(1-0)$  data taken with other telescopes have been scaled to the 22" beam of the IRAM 30m telescope at 2.6 mm.

Despite the large scatter in the  $\text{CI}/\text{CO}$  ratio, there is no apparent segregation between the different galaxy types. Viewed at large scale (the 15" CSO beam represents a linear scale of 730 pc at a distance of 10 Mpc), there are no clear differences between normal spirals, merger galaxies and even low metallicity galaxies, except maybe two regions in M 33. However, there are local differences within galaxies, which we examine in the following subsection. Because  $^{13}\text{CO}$  emission is low in active galaxies (e.g. Taniguchi and Ohyama 1998), we compare  $\text{CI}(1-0)$  with  $^{13}\text{CO}(2-1)$  in section 3.2. We then discuss the respective contributions of atomic carbon and carbon monoxide to the gas cooling in galaxies, and finally we compare the  $\text{CI}(1-0)$  emission of nearby galaxies with the CII and FIR emission at the same angular resolution.

### 3.1. Disk galaxies

We have mapped the north-east half of the major axis of the edge-on galaxy NGC 891, made a cut through the disk of NGC 6946, and observed points in the nucleus and in the disk of several other galaxies. We investigate the difference between galaxy nuclei and the disks, and between active regions in spiral arms and the general interstellar medium.

As a point of reference, we examine in Figure 4 the distribution of CI and CO lines in the Milky Way Galaxy, as observed by FIRAS on board COBE (Bennett et al. 1994). It is clear that for the Milky Way, CI(1-0) decreases less rapidly than the CO lines with Galactic radius, moving out along the Galactic plane. The decrease is steeper for CO(4-3) than for CO(2-1). Also, neutral carbon is more excited in the nucleus, as seen by the higher CI(2-1)/(1-0) emissivity ratio : 1.3 in the nucleus versus 0.5 in the disk. The  $7^\circ$  beam of COBE corresponds to a linear size of 1 kpc at the Galactic Center, quite similar to the linear size of the 15" CSO beam at a distance of 10 Mpc (0.7 kpc). Also shown in Figure 4 is the dust continuum at 1mm from the same COBE/FIRAS data. It is clear that the continuum intensity does not drop as fast as the CO and CI lines outside the nucleus of the Milky Way.

Figure 5 and 6 present a comparison of the CI(1-0) intensity with CO(1-0) in NGC 891 and NGC 6946 respectively. A similar effect to that seen in the Milky Way is seen for NGC 891, NGC 6946 and also for NGC 3079 : CI(1-0) is weaker, relative to CO(1-0) and (2-1), in the nucleus than in the disk. Toward NGC 891, we can compare CI(1-0) with both CO(1-0) and the dust continuum emission at 1.3mm from Guélin et al. (1993). Whereas the CI/dust continuum ratio stays constant throughout the disk, the CO/dust continuum increases, and the CI/CO decreases in the nucleus. Nuclear gas is usually denser and warmer

than the bulk of the interstellar gas in galactic disks, resulting in a higher excitation temperature for carbon monoxide in the nucleus. This difference in excitation has some consequences for the use of  $^{12}\text{CO}(1-0)$  as a tracer of molecular gas since the mass of molecular gas deduced from  $^{12}\text{CO}(1-0)$  data will be overestimated in galaxy nuclei. This has been shown for the Galactic Center by Sodroski et al. (1995).

For NGC 6946, the  $\text{CI}(1-0)/\text{CO}(2-1)$  ratio increases just outside the nucleus, in an interarm region, and decreases again when reaching a star forming region near the position  $(0, +140'')$ . For other galaxies also : M 33 (Wilson 1997), IC 10 (this work), a similar difference is found between clouds close to HII regions and clouds more distant from star forming complexes.  $\text{CI}(1-0)$  appears to be a tracer of the general interstellar medium, not strongly biased toward the densest and warmest places.

### 3.2. Comparison with $^{13}\text{CO}(2-1)$

In the Milky Way, a remarkable linear correlation between  $\text{CI}(1-0)$  and  $^{13}\text{CO}(2-1)$  intensities has been found in most of the clouds mapped (Keene et al. 1996). This correlation can be understood in the sense that both atomic carbon and  $^{13}\text{CO}$  are good tracers of the molecular gas given the permeability of the clouds to the UV radiation : the two lines have similar (moderate) opacities and are close to LTE for most of the physical conditions encountered in local molecular clouds. However, compared to maps of individual molecular clouds in the Milky Way, larger linear scales are sampled in external galaxies where the relation between CI and  $^{13}\text{CO}$  has not yet been studied. It is well known that  $^{13}\text{CO}$  lines are especially weak relative to  $^{12}\text{CO}$  in some interacting and merging galaxies (Casoli et al. 1992, Aalto et al. 1995, Taniguchi and Ohyama 1998).

We have therefore looked at possible variations of the CI/ $^{13}\text{CO}$ (2-1) ratio as a function of the  $^{13}\text{CO}$ (2-1) intensity. The data are displayed in Figure 7, with the same symbols as in Figure 3. We used  $^{13}\text{CO}$ (2-1) data from the literature as listed previously, or took new CSO data when needed.

This plot shows a trend of decreasing CI/ $^{13}\text{CO}$ (2-1) ratio with the  $^{13}\text{CO}$  intensity, with a few exceptions : M 33, the nucleus of Centaurus A and NGC 253. The trend is particularly clear for the disk of NGC 891 (black triangles in Fig. 7). Such a trend has been observed towards well known PDRs (Tauber et al. 1995, White & Sandell 1995, Minchin & White 1995). It can be understood as revealing a smooth variation of the abundance ratio N(C)/N(CO) with the total gas column density. Indeed, chemical models predict a decrease of the N(C)/N(CO) column density ratio with increasing H<sub>2</sub> column density in the range  $0.1 - 5 \times 10^{21} \text{ cm}^{-2}$ , valid for translucent clouds (Stark et al. 1996). If translucent gas represents a fair fraction of the molecular gas in external galaxies, atomic carbon lines will trace preferentially these physical conditions. As mentioned in the Introduction, from our knowledge of interstellar clouds in the Milky Way, it is expected that a significant fraction of the molecular gas is exposed to UV radiation. This seems to be the case in external galaxies as well since the CI(1-0) line at 492 GHz shows up at a detectable level in all types of galaxies, and does not show any peculiar behavior with the morphological type. Furthermore, in NGC 891, CI emission closely follows the dust continuum emission, which is also believed to be a reliable gas tracer in spiral galaxies. We conclude that CI(1-0) can be used as a tracer of low to moderate density molecular gas in external galaxies. It is possible that CI avoids the regions with high density, which represent a small fraction of the total gas mass of galaxies.

## 4. Gas cooling in galaxies

### 4.1. C and CO cooling

We have estimated the total cooling due to the observed lines of atomic carbon, CI(1-0), and carbon monoxide, CO(1-0) - (2-1) - (3-2) and in some cases (4-3). The data are reported in Table 3. It turns out that a significant fraction of the cooling is due to the CO(3-2) and (4-3) lines, so we report only a lower limit for CO cooling in galaxies with no CO(3-2) or (4-3) data. In order to estimate the total cooling due to all carbon and CO lines, we need to correct for the missing lines : CI(2-1) at 809 GHz, and CO(5-4), (6-5),... As templates, we used well studied cases, either the COBE data towards the Galactic Center or data on M 82 and IC 342 (Güsten et al. 1993). The correction for missing lines amounts, on average, to approximatively a factor 2 for carbon and a factor 4 for CO when no CO(4-3) and higher J data are available, or 2 when no CO(6-5) and higher J are available.

Israel et al. (1995) conclude that the contributions of CO and atomic carbon to the total cooling are similar for NGC 253. We show that this conclusion holds for all the galaxies in this sample. The contribution of CO and atomic carbon to the total cooling represent a small fraction of the total gas cooling, which is still dominated by CII, and possibly OI. Typically, the gas cooling due to atomic carbon or CO amounts to  $10^{-5}$  of the FIR dust continuum, while the gas cooling due to CII and OI amounts to  $10^{-4} - 10^{-2}$  of the FIR dust continuum.

### 4.2. Comparison with CII and FIR

We show in Figure 8 the line to continuum ratio CII/FIR versus CI(1-0)/FIR, and the line ratio CII/CI(1-0) versus CI(1-0)/FIR. The lines drawn in Figure

8 show PDR model predictions (using the code described in Le Bourlot et al. 1993) for hydrogen densities from  $10^2 \text{ cm}^{-3}$  to  $10^5 \text{ cm}^{-3}$  and  $G_0$  from 1 to  $10^4$  times the average radiation field in the solar neighborhood. The Far-infrared emission (FIR) is calculated from the measured fluxes at 60 and 100  $\mu\text{m}$ , available from observations with the Kuiper Airborne Observatory (Madden et al. 1997, 1998, Stacey et al. 1991, Smith and Harvey 1996) or with the Infrared Space Observatory (ISO) (Luhman et al. 1998) with the formula :  $FIR = 1.26 \times 10^{-14}(2.58F_{60} + F_{100})W\text{m}^{-2}$ , where  $F_{60}$  and  $F_{100}$  are the fluxes at 60 and 100  $\mu\text{m}$  in Janskys. Since the CII and FIR data have been taken at a lower spatial resolution than the CI data, we have smoothed or extrapolated the CI(1-0) data to a 55" beam, the spatial resolution of the CII and FIR data. For nearby spiral galaxies (NGC 891, NGC 6946), the data correspond to the central 55". The CII/CI(1-0) ratio shows a remarkable decreasing trend with increasing CI(1-0)/FIR ratio, except for the two ultraluminous infrared galaxies, Arp 220 and Mrk 231. The line to continuum ratio CII/FIR is also well correlated with CI(1-0)/FIR (Fig. 8) for all the studied galaxies, with the exceptions of Arp 220 and Mrk 231 which again lie significantly lower than the PDR model predictions.

These two plots can be understood as showing variations of the mean UV radiation field in the galaxy sample : for moderate UV illumination ( $G_0 = 10 - 100$ ), the gas heating due to the photoelectric effect on grains reaches maximum efficiency (Kaufman et al. 1999), so that the line to continuum ratios CI(1-0)/FIR and CII/FIR reach their maximum values. When the UV radiation field increases, the gas heating is less efficient, while the dust heating stays at the same level per UV photon. In that case, the far infrared radiation scales linearly with  $G_0$ , while the CII emission scales only logarithmically, and the

CI(1-0) emission stays nearly at the same level. The ratio CI(1-0)/FIR and CII/FIR are thus expected to decrease as  $G_0$  increases, and can be used to get estimates of the intensity of the radiation field in starburst galaxies. Because CI(1-0) is less sensitive than CII to  $G_0$  and the gas density  $n_H$ , a variation of the line ratio CII/CI(1-0) is predicted by PDR models (cf Figure 1), which explains the trends seen in Figure 8.

Most of the studied galaxies lie in the parameter space,  $G_0 = 10^2$  to  $10^3$ ,  $n = 10^2$  to  $10^5$ , as expected for molecular clouds in central regions of nearby galaxies. In M 82, a nearby starburst galaxy, the radiation field is more intense and reaches  $\sim 10^3$  in good agreement with the estimate given by Kaufman et al. (1999). The two merger galaxies, Arp 220 and Mrk 231 lie at the bottom left of the CII/FIR versus CI(1-0)/FIR plot, where both the radiation field and the gas density are high. For these extremely bright sources, the emission of individual PDR clouds can not be simply added as in nearby spiral galaxies and the opacity of the CII and OI lines (and possibly also the opacity of the dust thermal emission) must be taken into account as discussed in Gerin and Phillips (1998) and Luhman et al. (1998).

Because most of the PDR CII and CI(1-0) emission arises from the surface of molecular clouds, the filling factors of the CII, CI and FIR emission are expected to be similar for starburst galaxies. Furthermore, since CI(1-0) is less likely than CII to be contaminated by other emission sources (HII regions, WIM etc.), the CI(1-0)/FIR ratio is a better measure of  $G_0$  than the CII/FIR ratio. For star forming galaxies, where the dust heating is dominated by the radiation of massive stars, the line to continuum ratio CI(1-0)/FIR can thus be used to measure the strength of the UV radiation field. This conclusion is valid for spiral galaxies with the same metallicity as the Milky Way. In low metallicity galaxies,

the line and continuum emission do not scale the same way with metallicity and specific models must be used (Lequeux et al. 1994, Pak et al. 1998).

## 5. Conclusions

We have shown that the ground state fine-structure line of neutral carbon can be detected in a variety of external galaxies with current instrumentation. CI(1-0) data can be used in addition to other measurements to give information on the gas column density, the thermal balance and the UV illumination conditions in external galaxies. The results will be useful as templates for distant galaxies, when detectable with advanced instrumentation.

In nearby galaxies, atomic carbon is weaker relative to CO in the nucleus, but more widely distributed in the disk. This has important consequences for the thermal balance of the molecular interstellar medium. As a whole, the contribution of C and CO to the gas cooling are of the same order of magnitude :  $2 \times 10^{-5}$  of the FIR continuum or 5% of the CII line. C and CO cooling becomes significant, reaching  $\sim 30\%$  of the gas total, in merger galaxies like Arp 220 where CII is abnormally faint. This conclusion rests on the current data where only the ground state line of atomic carbon has been observed. Data on the second fine-structure line of atomic carbon at 809 GHz and on other CO lines are needed to obtain a better measurement of the gas cooling in galactic disks and nuclei.

We are grateful to F. Boulanger and G. Lagache for helping us using the COBE/FIRAS data. We thank J. Le Bourlot, G. Pineau des Forêts and E. Roueff for the use of their PDR model, and M. Guélin for sending us the continuum map of NGC 891. The CSO is funded by NSF contract AST96-15025.

M. Gerin acknowledges travel grants from INSU/CNRS, and NATO.

## REFERENCES

Aalto A., Booth R.S., Black J.H., Johansson L.E.B., 1995, A&A 300, 369.

Abgrall H., Le Bourlot J., Pineau des Forêts G., Roueff E., Flower D.R., Heck L., 1992, A&A 253, 525.

Baas F., Israel F.P., Koornneef J., 1994, A&A 284, 403

Bakes E.L.O., Tielens, A.G.G.M., 1998, ApJ 499, 258.

Becker R., PhD Thesis.

Bennett C.L., Fixsen D.J., Hinshaw G. et al., ApJ 434, 587.

Braine J., Guélin M., Dumke M., Brouillet N., Herpin F., Wielebinski R., 1997, A&A 326, 963.

Buat V., Burgarella D. 1998, A&A 334, 772.

Büttgenbach T.H., Keene J., Phillips T.G., Walker C.K., 1992, ApJ 397, L15.

Casoli F., Clausset F., Combes F., Viallefond F., Boulanger F., 1990, A&A 233, 357.

Casoli F., Dupraz C., Combes F., 1992, A&A 264, 55

Colbert J.W., Malkan M.A., Clegg P.E. et al., 1999, ApJ 511, 721.

Frerking M.A., Keene J., Blake G.A., Phillips T.G., 1989, ApJ 344, 311.

Garcia-Burillo S., Guélin M., Cernicharo J., Dahlem M., 1992, A&A 266, 21.

Garcia-Burillo S., Guélin M., Cernicharo J., 1993, A&A 274, 123.

Gerin M., Casoli F., Combes F., 1991, A&A 251, 32.

Gerin M., Phillips T.G., 1997, *The Far Infrared and Submillimetre Universe*, ESA SP-401, p 105.

Gerin M., Phillips T.G., 1998, ApJ 509, L17.

Guélin M., Zylka R., Mezger P.G., Haslam C.G.T., Kreysa E., Lemke R., Sievers A.W., *A&A* 279, L37.

Güsten R., Searbyn E., Kasemann C. et al., 1993, *ApJ* 402, 537.

Harrison A., Puxley P., Russel A., Brand P., 1995, *MNRAS* 277, 413.

Israel F.P., van Dishoeck E.F., Baas F., De Graauw T., Phillips T.G., 1991, *A&A* 245, L13.

Israel F.P., Tilanus R.P.J., Baas F., 1998, *A&A* 339, 398.

Israel F.P., White G.J., Baas F., 1995, *A&A* 302, 343.

Jenkins E.B., Shaya E.J., 1979, *ApJ* 231, 55.

Kaufman M.L., Wolfire M.G., Hollenbach D.J., Luhman M.L., 1999 *ApJ* submitted.

Keene J., Lis D.C., Phillips T.G., Schilke P., 1996, *IAU* 178, p 129.

Le Bourlot J., Pineau des Forêts G., Roueff E., Flower D.R., 1993, *A&A* 267, 233.

Lequeux J., Le Bourlot J., Pineau des Forêts G., Roueff E., Boulanger F., Rubio M., 1994, *A&A* 292, 371.

Liszt H.S., 1992, *ApJ* 386, 139.

Luhman M.L., Satyapal S., Fisher J., Wolfire M.G., Cox P., Lord S.D., Smith H.A., Stacey G.J., Unger S.J., 1998, *ApJ* 504, L11.

Mathis J.S., Mezger P.G., Panagia, N. 1983, *A&A* 128, 212.

Minchin N.R., White G.J., 1995, *A&A* 302, L25.

Pak S., Jaffe D.T., van Dishoeck E.F., Johansson L.E.B., Booth R., 1998, *ApJ* 498, 735.

Petitpas G.R., Wilson C.D., 1998, ApJ 503, 219.

Phillips T.G., Huggins P.J, 1981, ApJ 251, 533.

Plume R., Jaffe D.T., Tatematsu K., Evans N.J., Keene J., 1999, ApJ 512, 768.

Radford S.J.E., Downes D., Solomon P.M., 1991, ApJ 368, L15

Sauty S., Gerin M., Casoli F., 1998, A&A 339, 19.

Schilke P., Carlstrom J.E., Keene J., Phillips T.G., 1993, ApJ 417, L67.

Smith B.J., Harvey P.M., 1996, ApJ 468, 139.

Sodroski T.J., et al., 1995, ApJ 452, 262.

Solomon P.M., Downes D., Radford S.J.E., Barrett J.W., 1997, ApJ 478, 144.

Stacey G.J., Geis N., Genzel R., 1991, ApJ 373, 423.

Starck A.A., Bolatto A.D., Chamberlin R.A., Lane A.P., Bania T.M., Jackson J.M., Lo K., 1997, ApJ 480, L59.

Stark R., Wesselius P.R., van Dishoeck E.F., Laureijs R.J., 1996, A&A 311, 282.

Stutzki J., Graf U.U. et al., 1997, ApJ 477, L33.

Tauber J., A., Lis D.C., Keene J., Schilke P., Büttgenbach T.H., 1995, A&A 297, 567.

Tielens A.G.G.M., Hollenbach D., 1985, ApJ 291, 722.

White G.J., Sandell G., 1995, A&A 299, 179.

Wilson C.D., 1997, ApJ 487, L49.

## FIGURE CAPTIONS

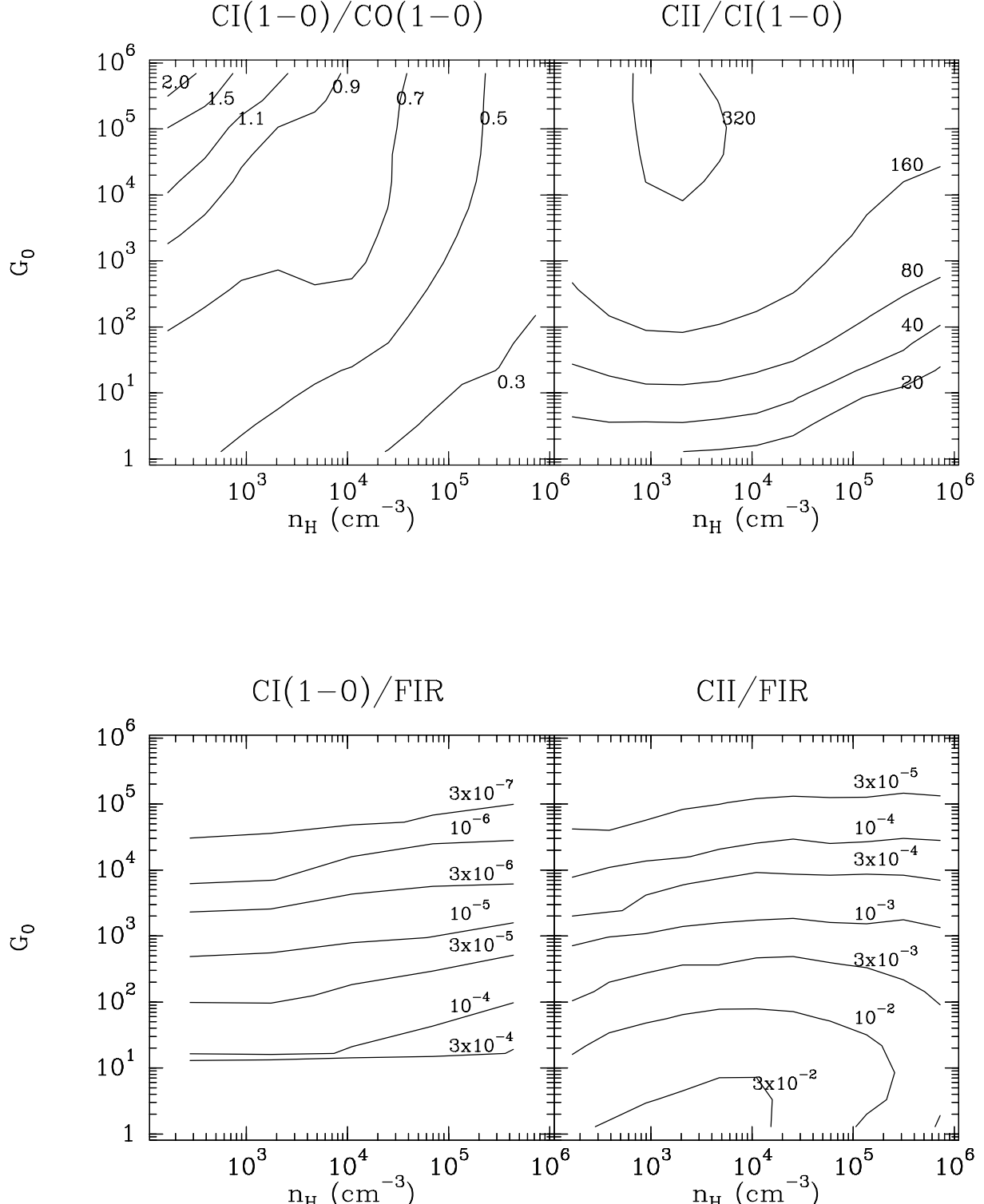
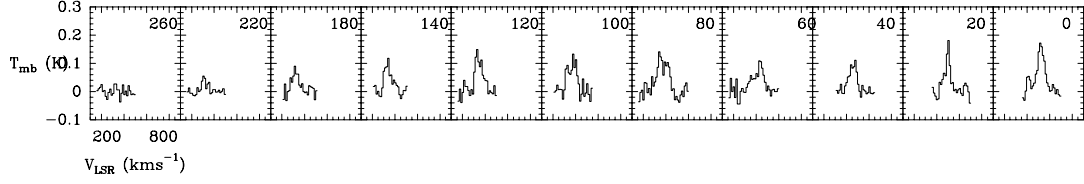


Fig. 1.— (Top left): Comparison of the intensity ratio  $\text{CI}(1-0)/\text{CO}(1-0)$  (in  $\text{Kkm s}^{-1}$ ) for a face-on PDR as functions of the uniform gas density  $n_H$  and UV illumination factor  $G_0$ . Contours are drawn at 0.3, 0.5, 0.7, ... 2. (Top Right) : Same comparison for  $\text{CII}/\text{CI}(1-0)$  (in  $\text{erg cm}^{-2}\text{s}^{-1}\text{sr}^{-1}$ ). Contours are drawn at 20, 40, 80, 160, ... 640. (Bottom left) : Same

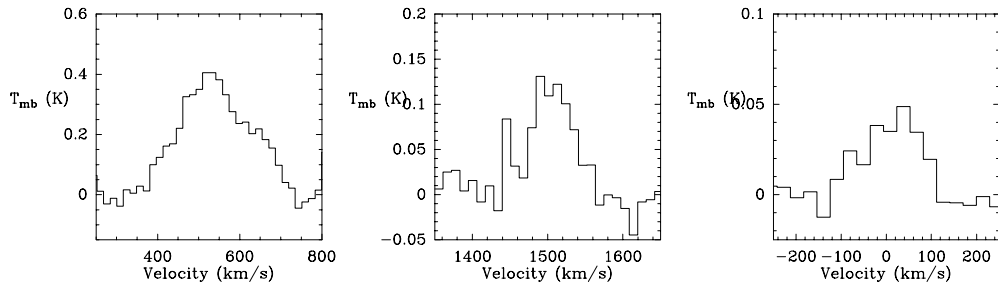
NGC 891



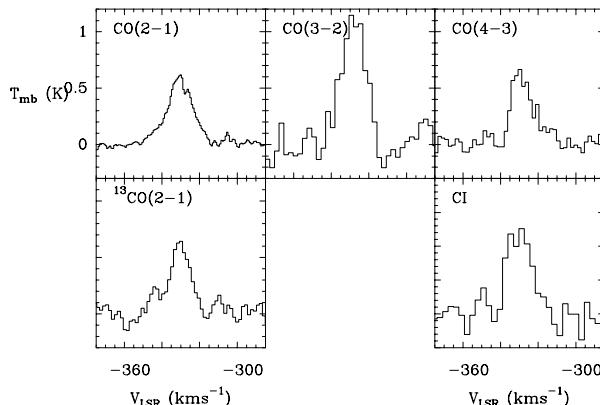
Centaurus A

NGC 4038/4039

Mrk 231



IC 10 (5,-20)



NGC 6946 (150,-20)

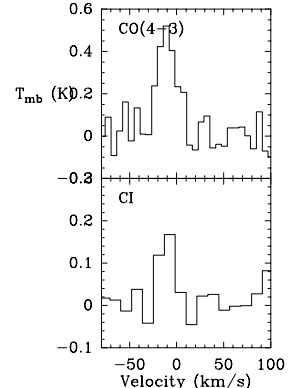


Fig. 2.— A selection of CSO spectra. (Top) : CI(1-0) data taken along the disk of NGC 891, (Middle) : Centaurus A (central region), The Antennae (overlap region) and Markarian 231, , (Bottom) : CO(2-1), (3-2), (4-3),  $^{13}\text{CO}$ (2-1) and CI(1-0) towards the nucleus of IC 10 (offsets (5",-20") from the position in Table 1), CO(4-3) and CI in a star forming complex in the disk of NGC 6946 (offsets (150",-20") from the position in Table 1). The temperature

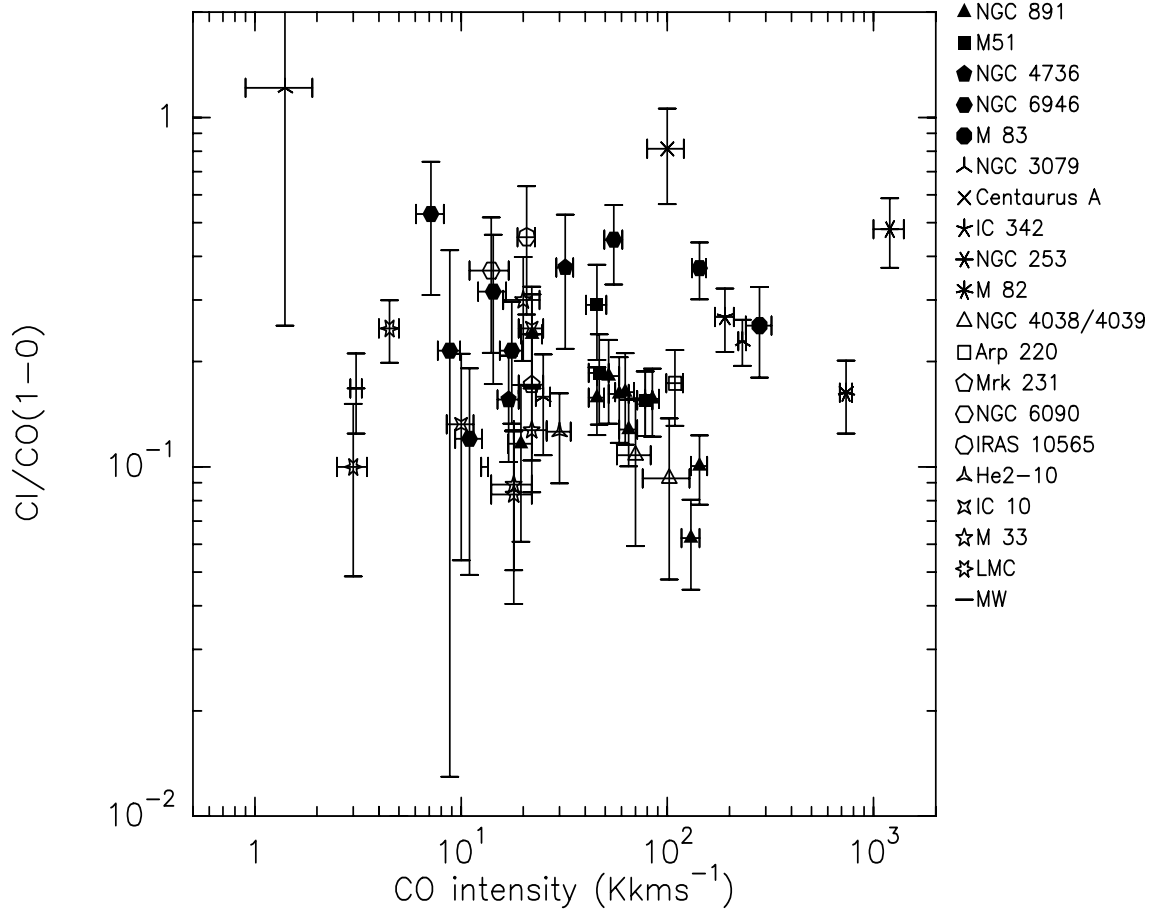


Fig. 3.— CI(1-0)/CO(1-0) Intensity ratio in  $\text{Kkm}^{-1}$  as a function of the CO(1-0) intensity in a 22" beam. The line intensities are given in  $T_{mb}$ . Different markers are used according to the galaxy type : black markers for normal spirals, cross-like for starburst and active galaxies, white for merger and interacting galaxies, and star-like markers for low metallicity galaxies. There is no obvious grouping by galaxy type in this presentation.

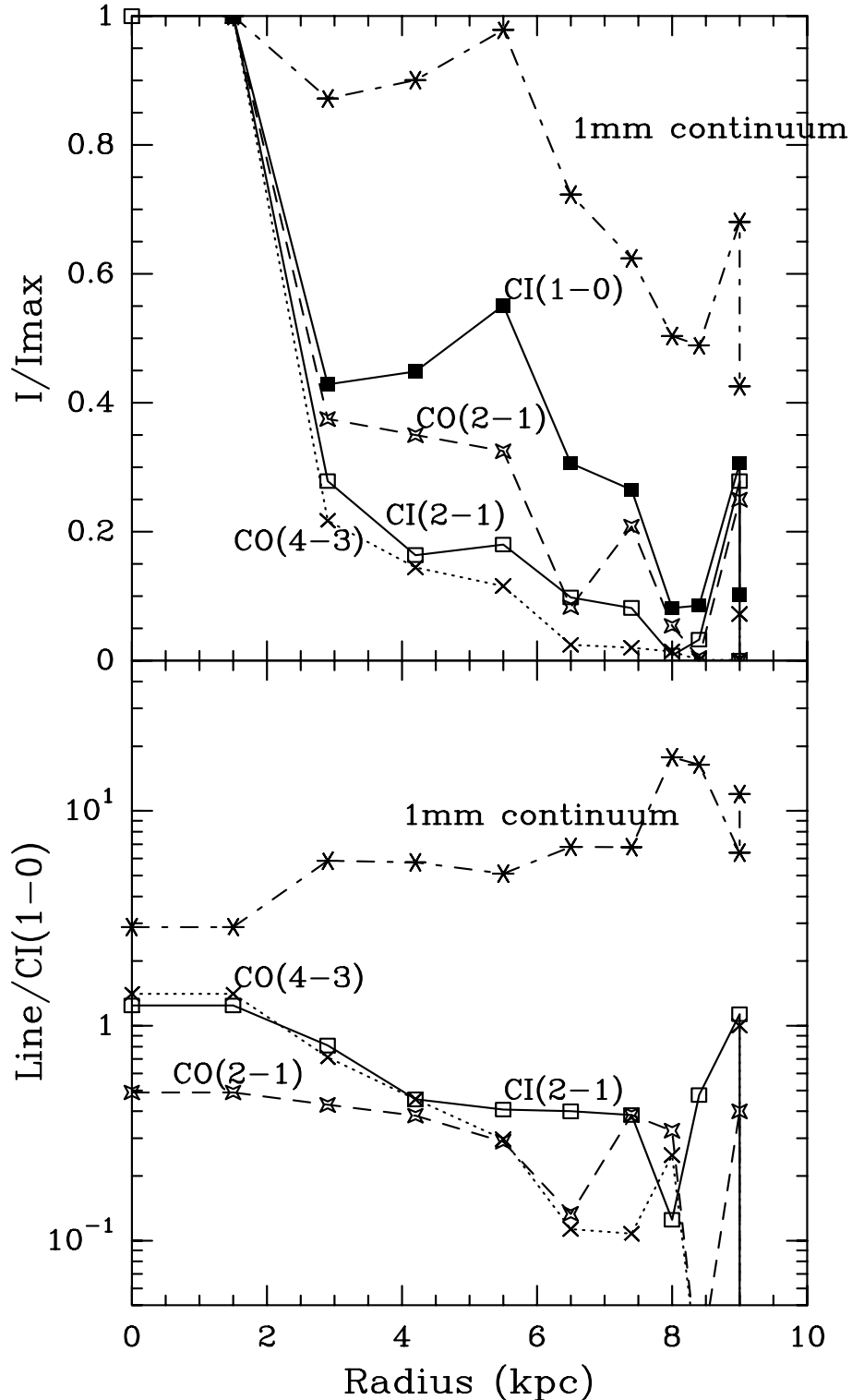


Fig. 4.— Upper : Distribution of the CI(1-0) (bold line, black squares), CI(2-1) (thin line, white squares), CO(2-1) (dashed line, stars) and CO(4-3) (dotted line, crosses) along the Galactic plane from COBE-FIRAS data. The 1mm continuum intensity is also shown for comparison (dotted-dashed line with stars). The intensity is normalized to the peak intensity

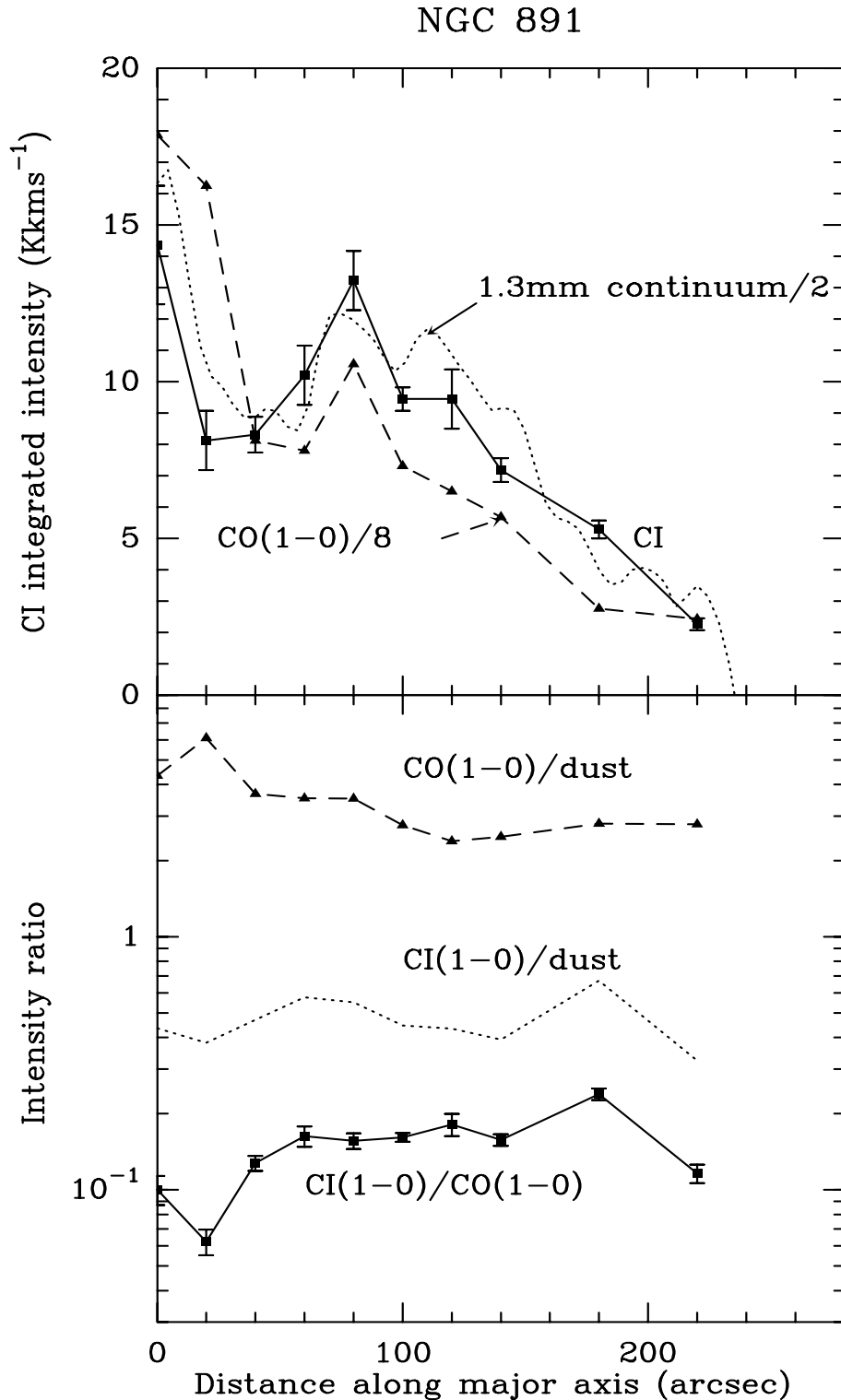


Fig. 5.— Upper : Distribution of the CI(1-0) (full line), CO(1-0) (dashed line, Garcia-Burillo et al. 1992) and dust continuum (dotted line, Guélin et al. 1993) along the major axis of NGC 891. The units of CI and CO(1-0) are  $\text{K km s}^{-1}$  and the dust continuum is in mJy. Lower : Intensity ratios along the major axis of NGC 891.

NGC 6946

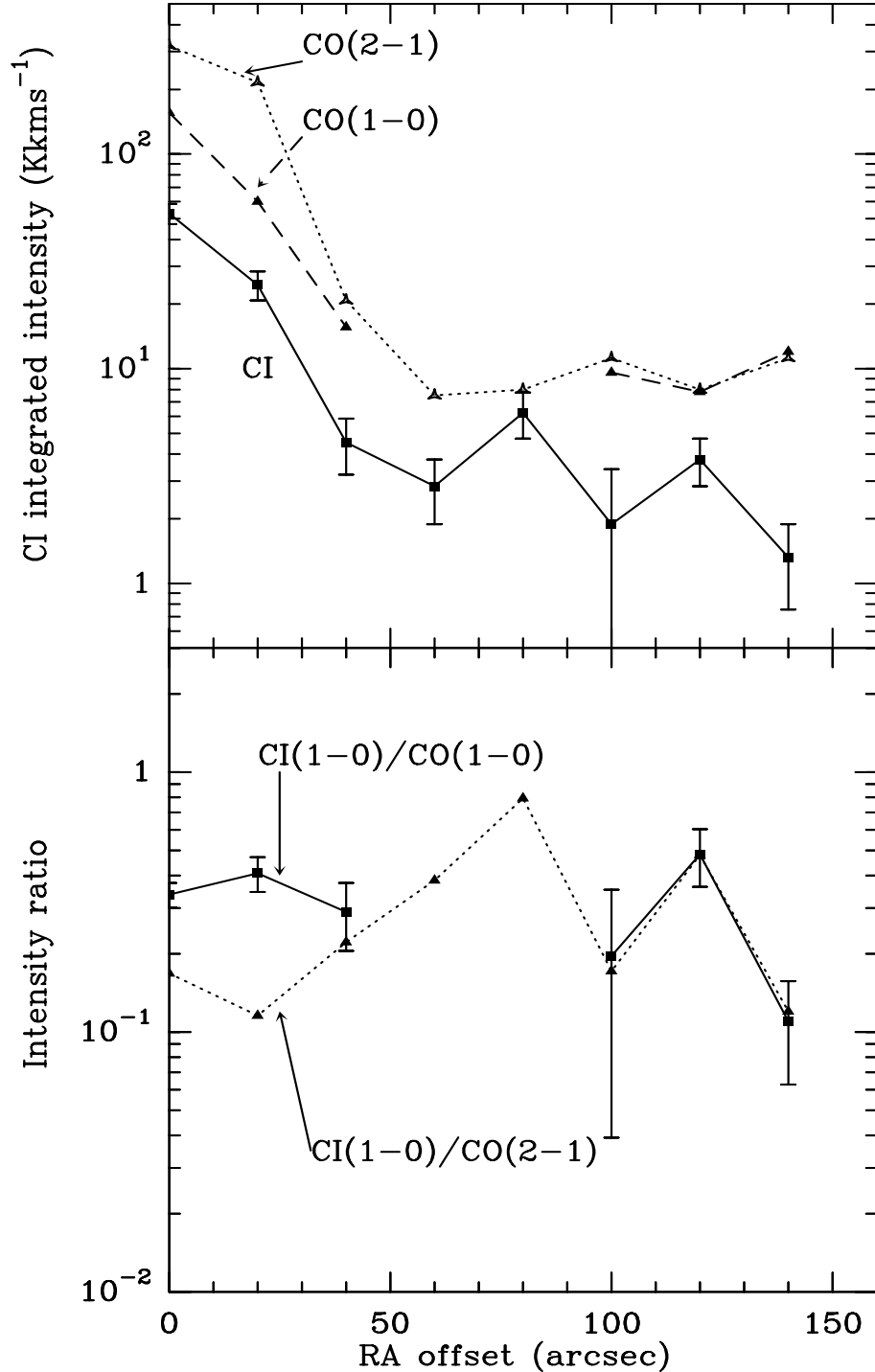


Fig. 6.— Upper : Distribution of the CI(1-0) (full line), CO(1-0) (dashed line, Casoli et al. 1990) and CO(2-1) (dotted line, Sauty et al. 1998) in the disk of NGC 6946. Lower : Intensity ratio for these lines.

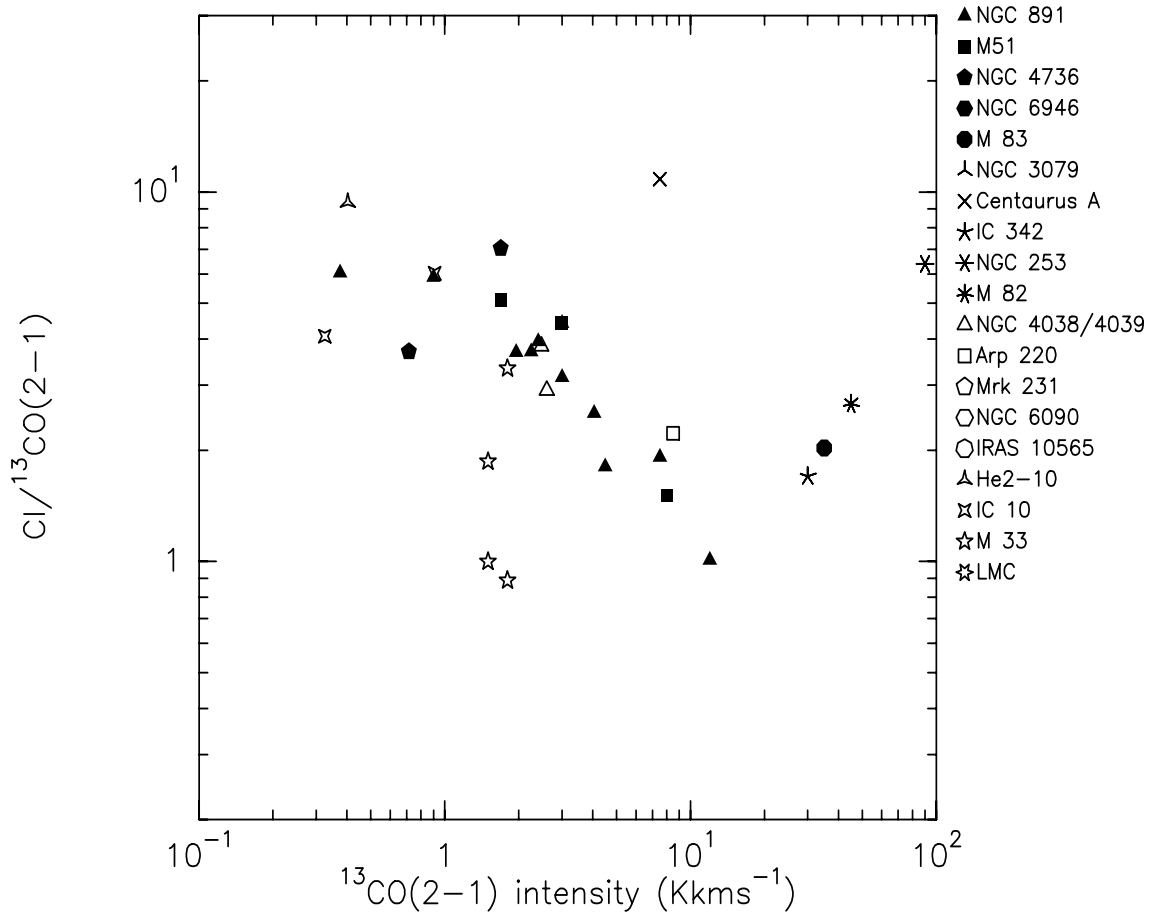


Fig. 7.—  $\text{CI}/^{13}\text{CO}(2-1)$  intensity ratio as a function of the  $^{13}\text{CO}(2-1)$  intensity. Symbols are the same as for Fig. 3.

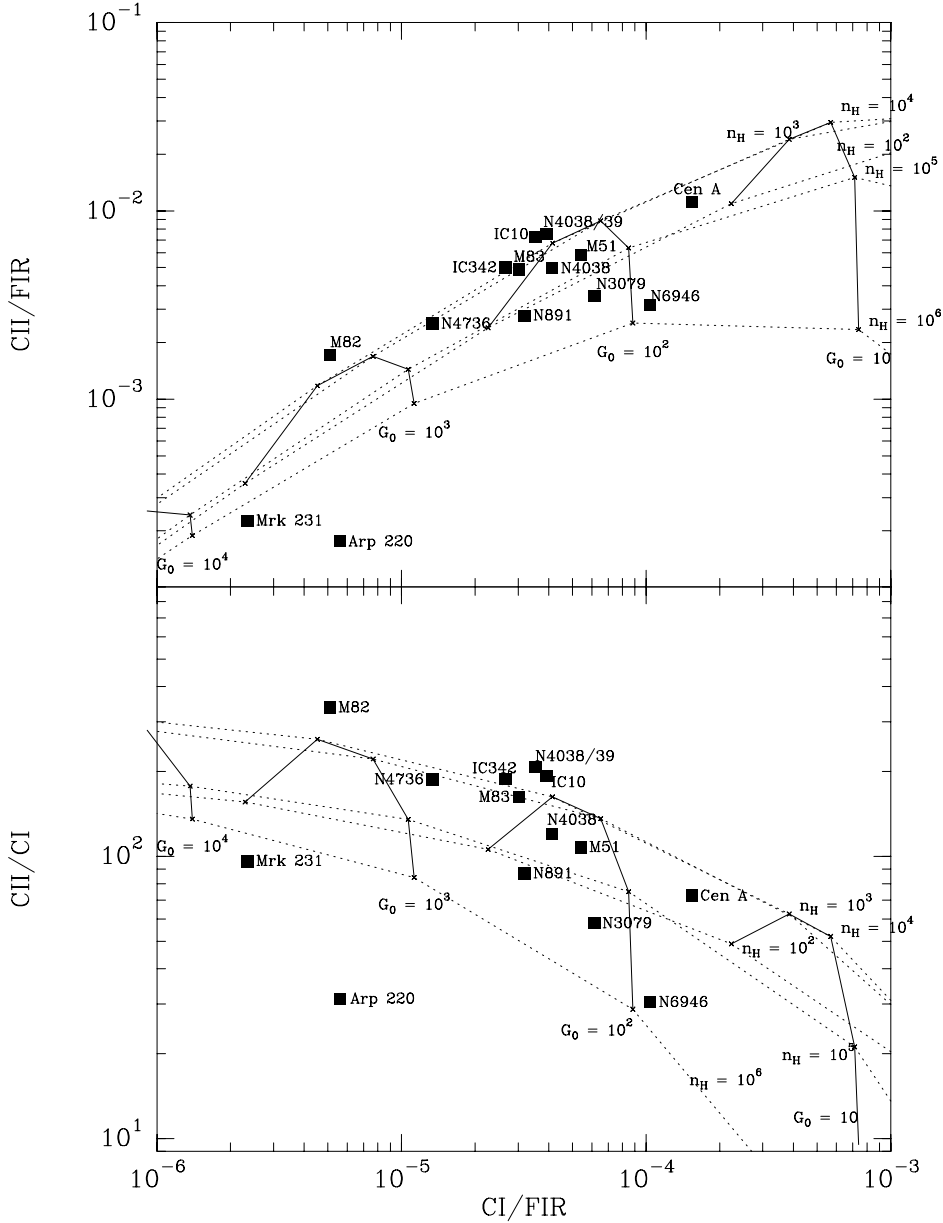


Fig. 8.— Line to continuum ratio CII/FIR (upper) and line emissivity ratio CII/CI (lower) versus CI/FIR in a 55" beam. The lines show PDR model predictions for  $n_H = 10^2$  to  $10^5$   $\text{cm}^{-3}$ , and  $G_0 = 10$  to  $10^4$ . The full lines are for constant  $G_0$ ; the dashed lines for constant density.

**Table 1:** Parameters of the observed sources

Name	Type	RA(1950)	Dec (1950)	$V_{LSR}$ (cz)	D(Mpc)	Comments
kms <sup>-1</sup>						
NGC 891	Sb	02:19:24.7	42:07:18.6	535	9.5	11 positions
NGC 3079	S	09:58:35.0	55:55:15.4	1331	16	3 positions
NGC 4736	Sab	12:48:31.9	41:23:31.2	314	5	2 positions
M 51	Sb	13:27:46.1	47:27:14	470	9.6	4 positions
NGC 6946	Sc	20:33:48.8	59:58:50.0	50	5	10 positions
Centaurus A	E/Irr	13:22:31.65	-42:45:32	550	3	Nucleus
NGC 4038	Int.	11:59:19.0	-18:35:23	1634	21	Nucleus
NGC 4038/4039	Int.	11:59:21.1	-18:36:17	1510	21	overlap region
Mrk 231	Merger	12:54:05.0	57:08:39	12650	170	
Arp 220	Merger	15:32:46.9	23:40:08	5450	77	
NGC 6090	Int.	16:10:24.0	52:35:11.0	8831	115	
IRAS10565+2448	Merger	10:56:36.2	24:48:40	12923	165	
IC 10	Irr	00:17:44.0	59:00:48	-344	1	2 positions
He 2-10	Irr	08:34:07.2	-26:14:06	873	9.2	Nucleus

Table 2: CI(1-0), CO(1-0) and  $^{13}\text{CO}$ (2-1) observed line strengths

Source	offset	CI (1-0)	CO(1-0)	$^{13}\text{CO}$ (2-1)	Ref
	arcsec	$\text{Kkm s}^{-1}$	$\text{Kkm s}^{-1}$	$\text{Kkm s}^{-1}$	
NGC 891	0	$14.4 \pm 1.9$	$143 \pm 13$	$7.0 \pm 1.4$	1
	20	$8.1 \pm 1.5$	$130 \pm 13$	$4.2 \pm 0.7$	1
	40	$8.3 \pm 1.0$	$70 \pm 6$	$2.1 \pm 0.4$	1
	60	$10.2 \pm 1.9$	$62 \pm 6$	$3.8 \pm 0.7$	1
	80	$13.2 \pm 1.9$	$84 \pm 6$	$2.8 \pm 0.7$	1
	100	$9.4 \pm 1.5$	$58 \pm 6$	$2.2 \pm 0.3$	1
	120	$9.4 \pm 1.3$	$52 \pm 6$	$2.8 \pm 0.7$	1
	140	$7.2 \pm 1.0$	$46 \pm 4$	$1.7 \pm 0.3$	1
	180	$5.3 \pm 1.0$	$22 \pm 3$	$0.9 \pm 0.2$	1
	220	$2.3 \pm 0.8$	$20 \pm 3$	$0.4 \pm 0.1$	1
	260	$0.2 \pm 0.2$	$10 \pm 3$	$0.3 \pm 0.3$	1
M 51	0,0	$13 \pm 2$	$45 \pm 5$		2
	-24,-24	$12 \pm 1.5$	$78 \pm 7$		2
	0,12	$9 \pm 1.5$	$47 \pm 5$		2
NGC 4736	0,0	$12 \pm 4$	$32 \pm 3$	$1.8 \pm 0.7$	3
	40,0	$2.6 \pm 0.6$	$17 \pm 2$	$0.8 \pm 0.15$	3
NGC 3079	0,0	$53 \pm 6$	$231 \pm 10$	$\pm$	4
	10,-50	$4.0 \pm 1.0$	$25 \pm 2$	$\pm$	4
	-35,130	$1.7 \pm 0.5$	$1.4 \pm 0.5$	$\pm$	4

Source	offset	CI (1-0)	CO(1-0)	$^{13}\text{CO}(2-1)$	Ref
		$\text{Kkm s}^{-1}$	$\text{Kkm s}^{-1}$	$\text{Kkm s}^{-1}$	
NGC 6946	0,0	$53 \pm 5.7$	$150 \pm 12$	$\pm$	5
	20,0	$25 \pm 3.8$	$60 \pm 6$	$\pm$	5
	40,0	$4.5 \pm 1.3$	$16 \pm 2.5$	$\pm$	5
	60,0	$2.8 \pm 1.0$	$\pm$	$\pm$	5
	80,0	$6.2 \pm 1.5$	$\pm$	$\pm$	5
	100,0	$1.9 \pm 1.5$	$9.6 \pm 1.2$	$\pm$	5
	120,0	$3.8 \pm 1.0$	$7.8 \pm 1.2$	$\pm$	5
	140,0	$1.3 \pm 0.6$	$12 \pm 1.8$	$\pm$	5
	150,-20	$3.8 \pm 1.0$	$19 \pm 2.4$	$\pm$	5
	110,100	$4.2 \pm 1.0$	$\pm$	$\pm$	5
He 2-10	0,0	$3.8 \pm 0.6$	$30 \pm 4$	$0.4 \pm 0.1$	6
IC 10	5,-20	$5.5 \pm 1.0$	$22 \pm 3$	$1.0 \pm 0.15$	7
	-30,240	$1.3 \pm 0.6$	$10 \pm 1.5$	$0.35 \pm 0.07$	7
NGC 4038/39	overlap	$9.5 \pm 1.9$	$102 \pm 20$	$2.7 \pm 0.4$	8
NGC 4038	0,0	$7.6 \pm 1.9$	$70 \pm 10$	$2.8 \pm 0.7$	8
Arp 220		$19 \pm 2.8$	$109 \pm 10$	$8.5 \pm 1$	9
Mrk 231		$3.8 \pm 1.0$	$22 \pm 3$	$\pm$	10
NGC 6090		$5.1 \pm 1.0$	$14 \pm 3$	$\pm$	11
IRAS 10565+2448		$9.5 \pm 2.8$	$16 \pm 2$	$\pm$	10
Centaurus A	0,0	$81 \pm 7.6$	$100 \pm 20$	$7.5 \pm 3.0$	12

(1) Garcia-Burillo et al. (1992), (2) Garcia-Burillo et al. (1993), (3) Gerin et al. (1991), (4) Braine et al. (1997), (5) Casoli et al. (1990), (6) Baas et al. (1994), (7) Becker (1992), (8) Aalto et al. (1995), (9) Radford et al. (1991), (10) Solomon et al. (1997), (11) Liszt (1992), (12) Israël et al. (1991)

Table 3: Contribution of CI(1-0) and CO lines to the thermal balance

Source	CI (1-0)	CO <sup>1</sup>	FIR
	$10^{-17} \text{ Wm}^{-2}$	$10^{-17} \text{ Wm}^{-2}$	$10^{-12} \text{ Wm}^{-2}$
NGC 891 - Center	1.2	2.4	4.5
NGC 891 - (100" NE)	0.82	1.3	
M 51* - Center	1.1	3.3	6.7
M 51* - (-24",-24")	1.0	2.6	
NGC 4736 - Center	1.0	2.0	3.7
NGC 4736 - (40",0)	0.23	0.95	
NGC 6946* - Center	4.6	21	8.8
NGC 6946 - (150",-20")	0.33	1.1	
NGC 3079 - Center	4.6	$\geq 2.1$	2.9
NGC 3079 - (-35",130")	0.15	$\geq 0.02$	
He2-10	0.33	1.1	1.1
IC 10*	0.48	2.3	2.0
Centaurus A	7.1	6.1	13.4
NGC 4038/4039	0.82	3.9	2.2
NGC 6090	0.44	1.2	0.33
Arp 220	1.6	2.7	4.7
Mrk 231	0.33	0.56	1.4

<sup>1</sup> total CO flux from observed lines : (1-0), (2-1), (3-2) and (4-3) when available.

Galaxies with CO(4-3) data are indicated with an asterisk.